Chapter 6

EXPERIMENTAL DEMONSTRATION OF ISA CONCEPT

This chapter includes both published work from the following proceedings and new, unpublished sections:

J. Suh, S. P. Dassanayake, and S. Pellegrino, "In-Space Assembly of Large Mesh Reflectors," in *AIAA SCITECH 2025 Forum [Accepted]*, 2025.

J. Suh, S. P. Dassanayake, M. Thomson, and S. Pellegrino, "Scalable Concept for Reflector Antenna Assembled in Space," in *AIAA SCITECH 2024 Forum*, 2024, p. 0823. DOI: 10.2514/6.2024-0823.

J. Suh, S. P. Dassanayake, M. Thomson, and S. Pellegrino, "In-Space Assembly of Large Mesh Reflector Antennas," in *Aerospace Structures, Structural Dynamics, and Materials Conference, SSDM 2024 [Technical Presentation]*, 2024, p. 137 740.

J. Suh, S. Dassanayake, M. Thomson, and S. Pellegrino, "Concept for In-Space Assembly of Large Reflector Antennas," in *41st ESA Antenna Workshop ESTEC*, 2023.

6.1 Motivation

In parallel with the simulations described in Chapters 4 and 5, the DARPA NOM4D team (Dr. Jong-Eun Suh, Alan Truong and Charles Sommer) at the Space Structures Lab is constructing a lab-scale prototype to demonstrate the proposed ISA concept in space by 2026. This prototype features a twelve-sided reflector with a diameter of $D = 1.4$ meters. It is modularly designed and will be assembled using a truss builder prototype.

These experiments are crucial for validating the findings of the simulations. Specifically, these tests will help verify the accuracy of the two-dimensional simulation model in predicting the kinematics of the three-dimensional assembly process and evaluate whether the identified design considerations—such as assembly plate orientation, method of prestressing, and cable net orientation—are broadly applicable. This validation is particularly important given that future predictions about the kinematics of larger structures will rely on two-dimensional simulations.

This chapter compares the results from the lab-scale experiments with those from the simulations to evaluate the applicability and accuracy of the two-dimensional model in predicting the behavior of larger, more complex structures. This comparison will offer valuable insights into the reliability of the simulations and their potential for scaling to full-sized applications.

6.2 Design of In-Space Assembly Facility

To evaluate the feasibility of the proposed ISA concept, prototypes of each component, including the truss builder, have been manufactured and are currently being demonstrated in the laboratory. Figure 6.1 shows a CAD illustration of the target reflector. For an aperture size of 1.4 meters, the design outlined in Chapter 2 specifies $n = 4$ subdivisions of the reflective surface, which necessitates 12 bays for the perimeter truss. Since the truss builder substitutes the final bay of the perimeter truss, a total of 45 struts—comprising 22 longerons, 12 battens, and 11 diagonals—along with 24 joints, are required. The dimensions for the longeron, batten and diagonal (see Fig. 6.1(b)) are determined based on the geometry of a reflector with an F/D ratio of 1.0.

6.2.1 Lab-scale Reflector Prototype

Figure 6.2 illustrates the modular design of the reflector's structural components, intended for assembly by a simple robot, to minimize system complexity. A general overview of the reflector prototype is as follows. The joints are 3-D printed

using Polylactic Acid (PLA) with a CraftBot Plus Pro printer (see CAD image in Fig. 6.2(a)) and include bearings and torsional springs to provide rotation and stiffness.

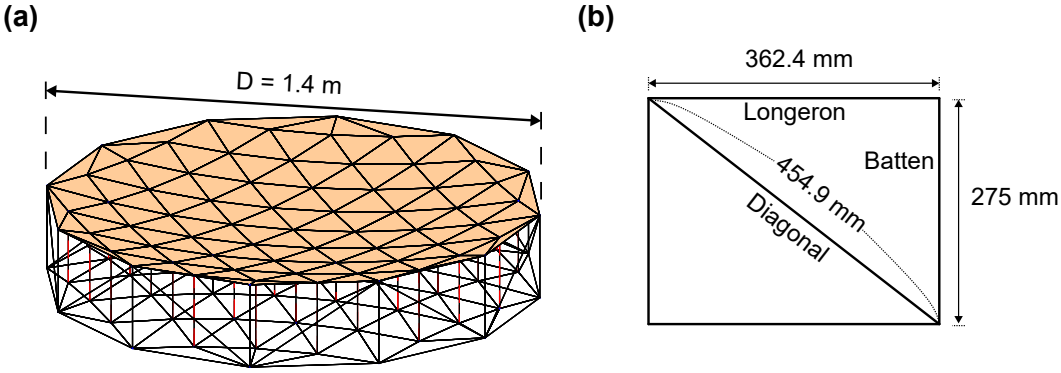

Figure 6.1: Lab-scale demonstration: a) target reflector, and b) dimensions of struts.

The initial prototype described here employs both permanent and electromagnets to secure the joints to the assembly plate. Each joint features recessed surfaces with permanent magnets to assist in aligning the struts. The struts, made from 6 mm diameter pultruded composite tubes, are equipped with magnetized caps that fit securely into these slots through a combination of friction and magnetic attraction, see Figs. 6.2(a) and (b). A circular permanent magnet, along with guiding cones, aids in mounting the joints on the assembly plate. The assembly plate is equipped with electromagnets that activate during bay construction and deactivate during bay release, enabling the connection between the joint and the assembly plate.

The cable net assembly for the mesh reflector includes a front and rear cable net and tension ties. The nets are made from 50 μm thick Kapton film, patterned with the design obtained for $D = 1.4$ m and $F/D = 1.0$, per Section 2.2.1. The front net has a Nylon knitted mesh attached underneath, and a push-latch device connects the nets to the perimeter truss joints, see Fig. 6.2(c). The tension ties, depicted in Fig. 6.2(d), consist of extension springs and strings and are used to maintain the tension of the net. The string length is specifically designed to achieve the necessary tension in the cable net assembly when fully deployed. The springs are sealed in rubber tubes to prevent tangling. The net prototype is stored in a fan-folded configuration within the truss builder. Before each bay release, the push-latch devices at the cable net nodes $C_{edge,\,i}$ are sequentially attached to the corresponding truss joints.

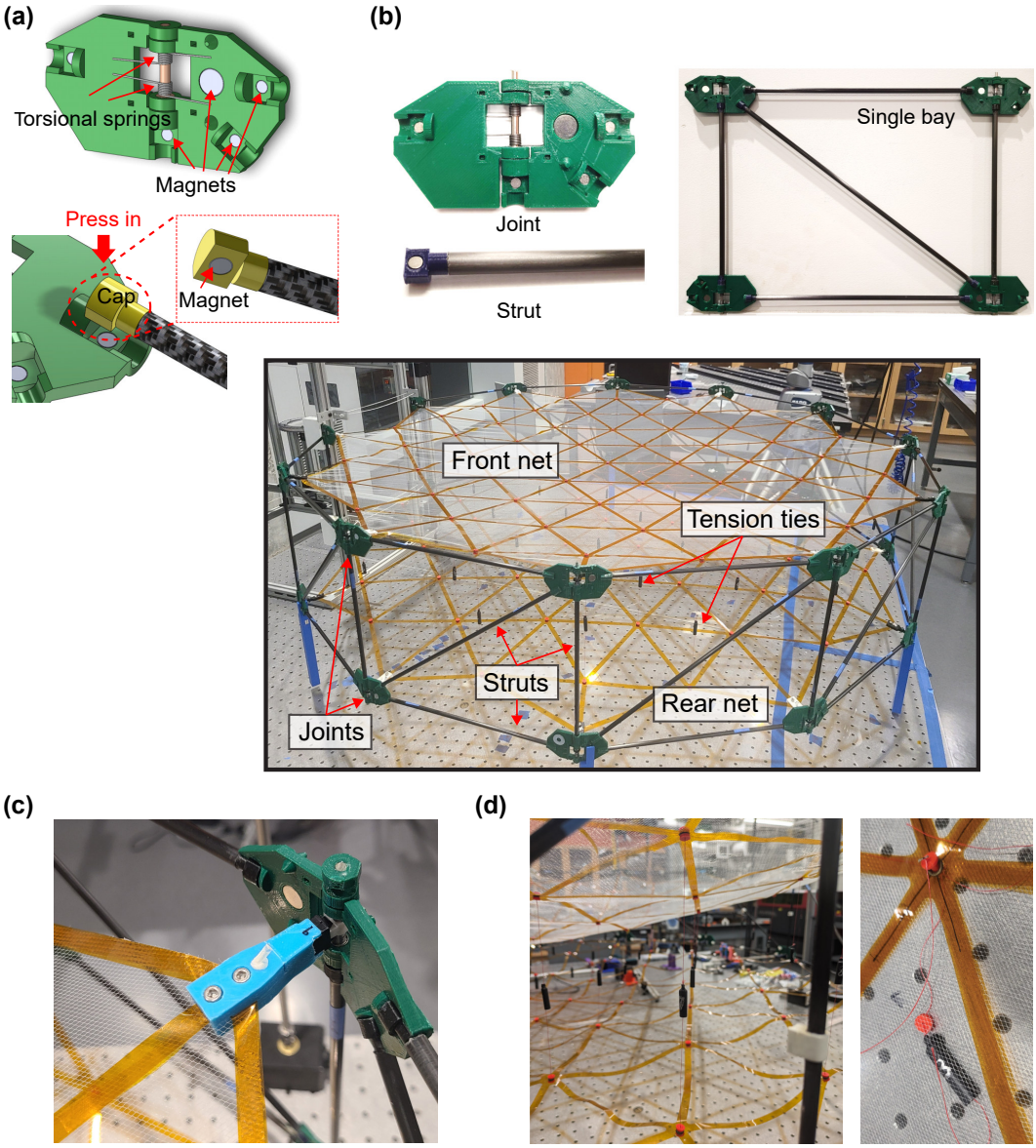

Figure 6.2: Reflector prototype, $D = 1.4$ m: a) CAD drawing of the joint and joint-strut attachment, b) prototypes of the joint, strut, and a single bay, and prototype of cable net with c) a push-latch device installed at the outer node of cable net and attached to the truss, and d) a tension tie.

6.2.2 Truss Builder Prototype

The truss builder prototype (Fig. 6.3(a)) consists of the following key components: the assembly plate, the strut storage, and the manipulator. It performs four major robotic operations, each supported by specific mechanical devices.

The sliding assembly plate handles the 'bay push-out and retraction,' while the joint mounting plates, equipped with electromagnets, secure the joints during

construction, facilitating the 'bay hold and release.' The 'bay construction' involves the joint and strut storage and is carried out by the manipulator, which has 4 DoF (translation in x, y, and z axes, and rotation in Rz). The manipulator, which includes two linear stages, a push actuator, and a rotator, positions the struts and joints from the storage onto the assembly plate (Fig. 6.3(c)). The strut storage is arranged around the perimeter of a circular drum, rotating to bring each strut to the pick-up position. The manipulator's electromagnet interacts with the permanent magnets in the strut sleeves to secure and release the struts. The sleeves are designed to prevent strut rotation during manipulation.

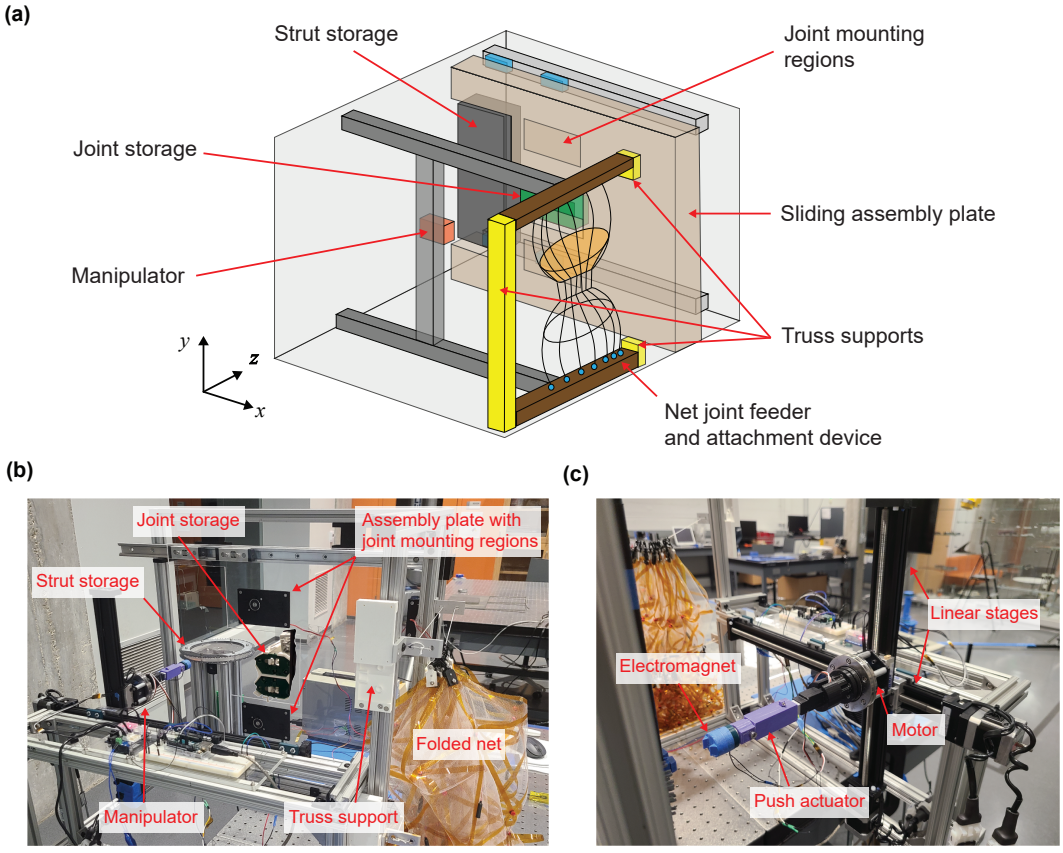

Figure 6.3: Truss builder prototype: a) schematic drawing of truss builder and components, and prototypes of: b) truss builder and c) manipulator.

The 'net attachment' is accomplished by a net joint feeder and attachment device, which organizes the push-latch devices in the order of truss assembly and attaches them to the corresponding truss joints before the assembly plate retracts.

Once a bay is assembled, electromagnets mounted in end fixtures at the edge of the truss builder (i.e., truss supports introduced in Chapter 4, see Fig. 6.3(a)) hold

the released bay, providing sufficient clearance for the assembly plate to retract for the next construction cycle. A prototype based on this design is shown in Figs. 6.3(b) and (c).

6.3 Design Considerations

Efforts were made to validate the design considerations identified from the two-dimensional simulations in Chapter 5. Specifically, two assembly plate orientations, $\theta = 90°$ and $\theta = 60°$, were tested, along with two prestressing methods: moving the last bay and adjusting the truss support. It was quickly determined that the cable net orientation 2 was the preferred option, as it effectively mitigated excessive tension in the cables, reducing the risk of damage during the assembly process. This orientation provided better control over the cable tension and structural integrity.

6.3.1 Angle Stops and Assembly Plate Orientation

In the first experiment with a 90° assembly plate, the structure was assembled manually. One critical difference between this experiment and the simulation was the absence of angle stops in this version of the prototype. Without these stops, the structure had the freedom to form concave polygons during assembly, which posed the risk of overstretching and potentially damaging the cables that support the structure, see Fig. 6.4(d). These kinks and deformations required manual intervention to correct the shape and ensure that the assembly could continue. This manual correction process, while effective for this test, underscored the crucial role of angle stops in automated operations. By constraining the structure's movement and preventing the formation of concave polygons, angle stops help to preserve the integrity of the cables and streamline the assembly process, ensuring that the structure deploys with greater precision and less risk of damage.

Figure 6.4(e) shows the final assembled reflector achieving the desired shape. However, it is important to note that this outcome is largely due to manual interventions, and the shape might not have been achieved without them.

In the $\theta = 60°$ experiment, the prototype featured angle stops and utilized a minimal-interference gravity offload system, where supports hoisted the structure at intermediate truss nodes using strings to ensure continuous vertical alignment. This setup effectively simulated a zero-gravity environment and minimized external forces that could distort the configuration. These enhancements significantly improved the precision of the deployment. As expected, the angle stops played a key role in controlling the structure's movement, preventing the formation of unwanted

kinks and concave polygons that were problematic in the $\theta = 90°$ case. With these mechanisms in place, the assembly process was smoother and more symmetrical (see Figs. 6.5(a-c)), enabling a more controlled deployment of each bay. The deployment was significantly more consistent and predictable compared to the earlier tests as well.

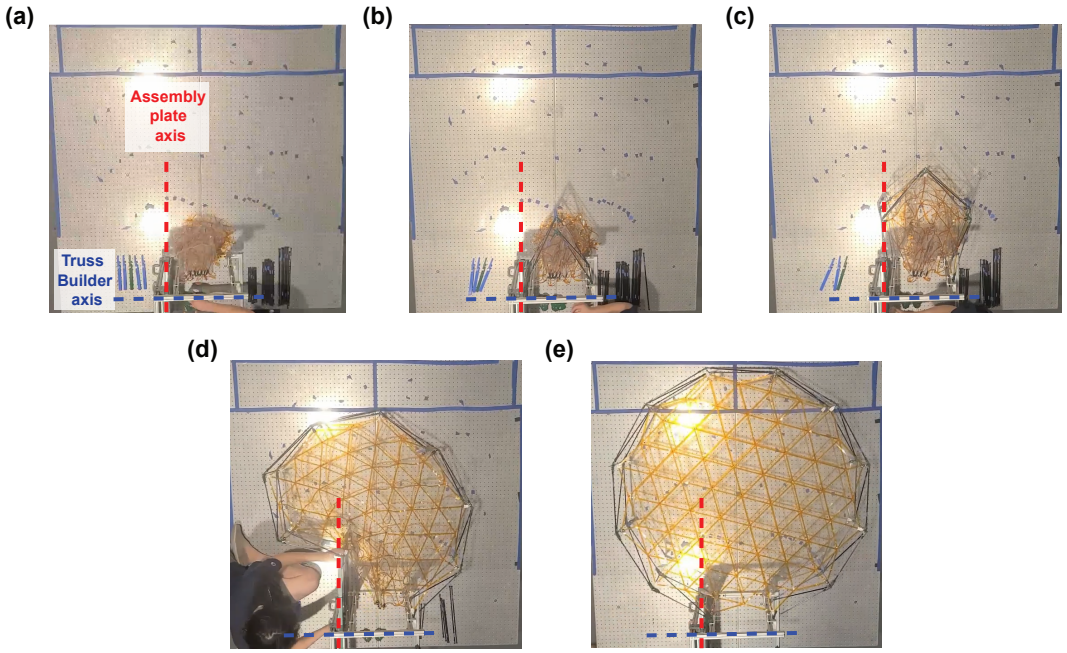

Figure 6.4: Reflector assembly demonstration for $\theta = 90°$: a) initial state, b) $i = 3$, c) $i = 5$, d) $i = 10$ with kink formation, and e) $i = 12$: completed reflector.

While the final assembled structure did not achieve good accuracy, the experimental results closely aligned with the expected configuration from the simulations, particularly towards the end of the assembly process, see Figs. 6.5(b) and (c). This agreement with the simulations confirmed the effectiveness of the design improvements, enabling smoother, more reliable assembly process and demonstrating that the structure could be successfully deployed with minimal intervention.

Simulations can be setup to follow any assembly plate angle between 0° and 90°. However, it is important to note that a smaller angle θ results in a reduced working space for the robotic manipulator, see Fig. 6.6. Therefore, a trial-and-error approach was used to determine a suitable angle between 90° and 60° that would offer more working space while ensuring an uninterrupted assembly process and achieving a shape closest to the desired one, ultimately selecting 72°.

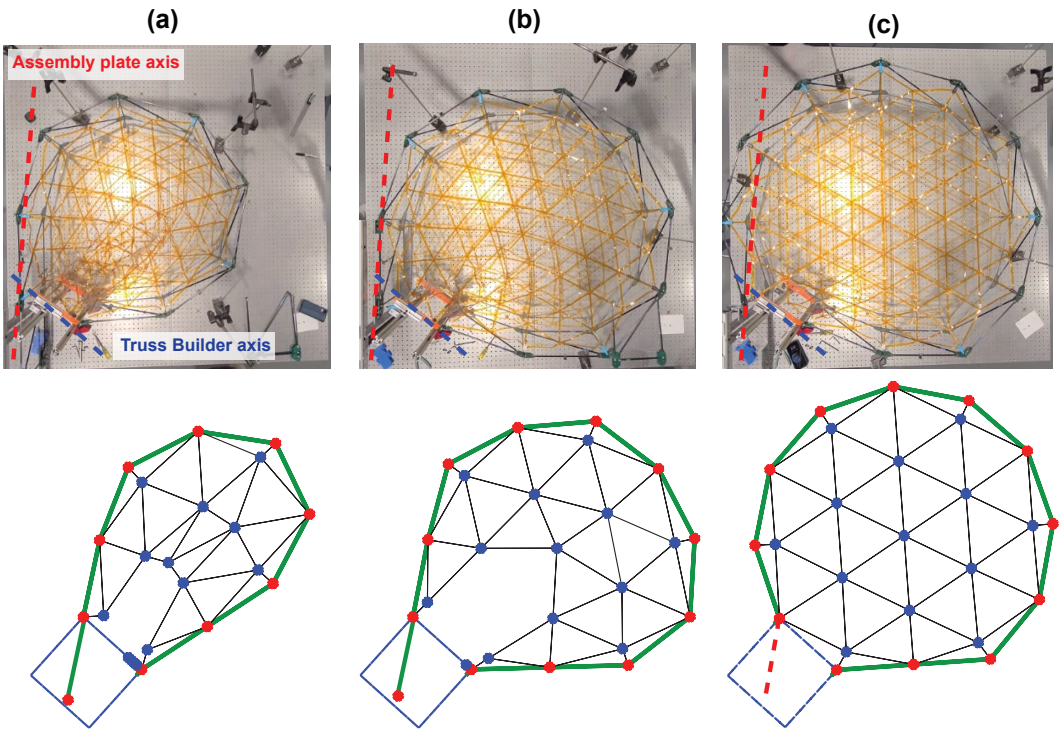

Figure 6.5: Comparison of experimental and simulation results for $\theta = 60°$: a) $i = 9$, b) $i = 11$, and c) $i = 12$: completed reflector.

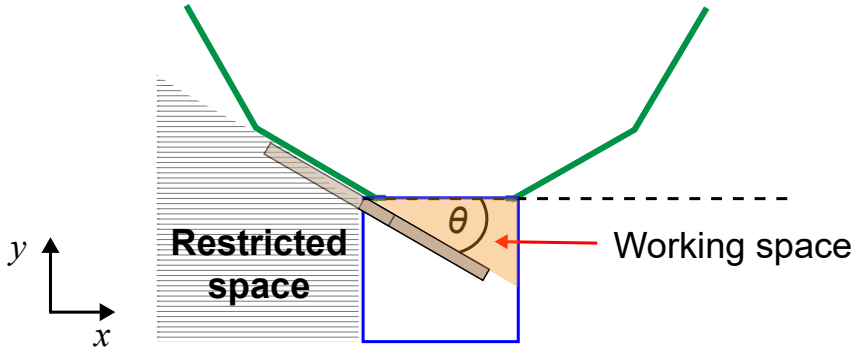

Figure 6.6: Relationship between θ and working space for the robotic manipulator.

6.3.2 Prestressing Method

The final configuration for the $\theta = 72°$ and cable net orientation 2, with prestressing achieved by moving the final bay as detailed in Section 5.3, shows that the nodes N_1-N_3 have become collinear (Fig. 6.7(a)), a result consistent with the simulations. A closer inspection reveals that the cable net is stretched undesirably due to the collinearity of the nodes when prestressing is achieved by moving the last bay, see Fig. 6.7(b). This observation underscores that the assembly plate ori-

entation is not the sole design consideration. The method of prestressing must also be addressed in the experimental setup, with cables remaining slack until the final stages of the assembly process to ensure smooth progression.

In the $\theta = 72^\circ$ case, with prestressing imposed by adjusting the truss support, the assembly process starts with deploying the pre-built bays. After forming the initial polygon, the support is repositioned (Figs. 6.8(a) and (b)). Despite noticeable distortion, the assembly proceeds smoothly as more bays are added, causing the reflector's diameter to gradually increase. The shape of the truss becomes biased away from the assembly plate (Fig. 6.8(c-e)). However, as the support is gradually moved back at the end of the assembly, the shape of the reflector is corrected (Fig. 6.8(f)), with the cable net near the first joint still exhibiting some sagging. The final configuration, shown with an overlay of the simulation results, demonstrates a good qualitative match, highlighting the effectiveness of the modification made to the prestressing method.

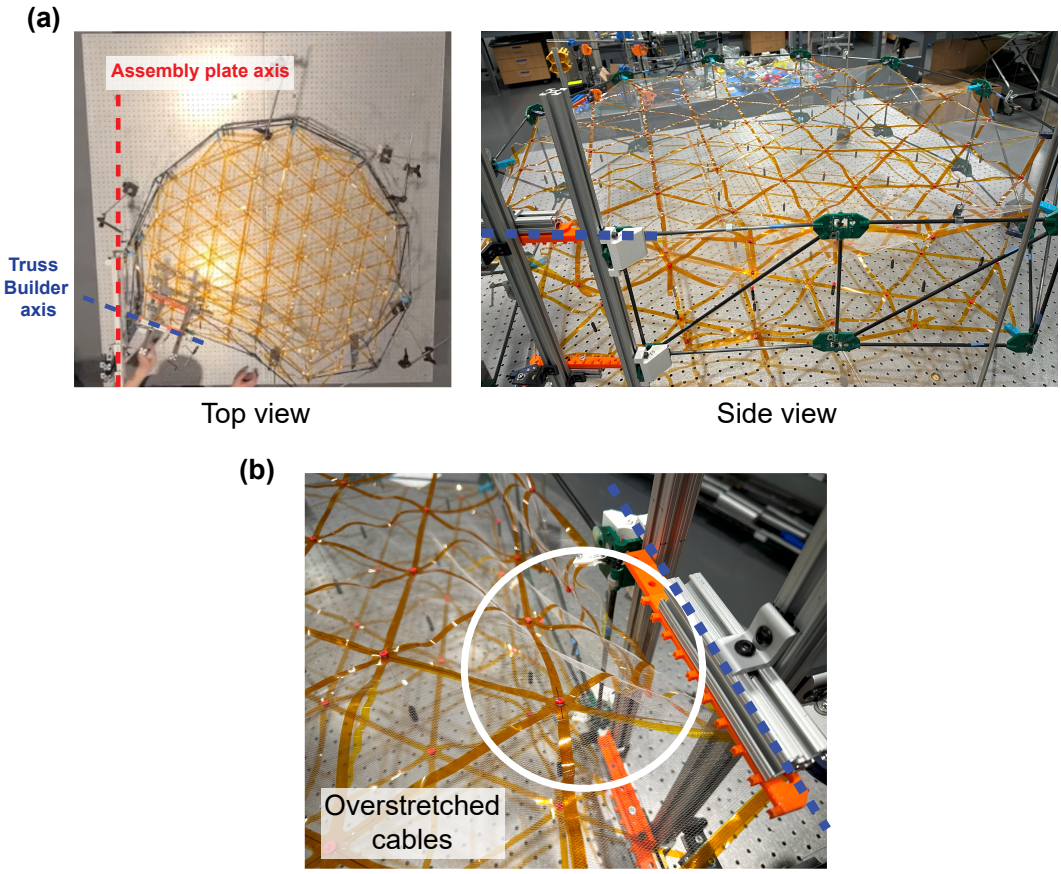

Figure 6.7: Reflector prototype assembled at $\theta = 72^\circ$, prestressed by moving the last bay: a) collinear truss nodes, and b) undesirable stretching of cables.

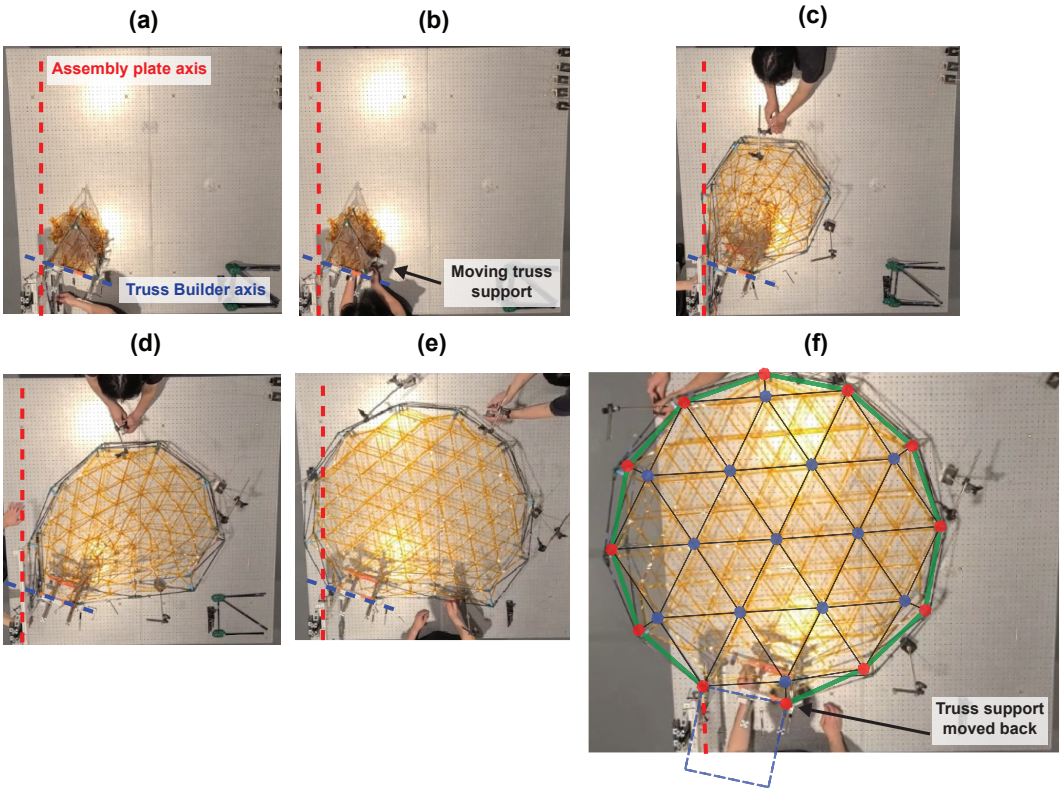

Figure 6.8: Assembly demonstration for $\theta = 72°$, prestressed by moving the truss support: a) $i = 3$, b) truss support S_1 moved, c) $i = 7$, d) $i = 10$, e) $i = 12$: prior to repositioning S_1, and f) $i = 12$: completed reflector, overlaid with the corresponding simulation result.

Based on these observations, a 72° assembly plate orientation was selected for future work on the prototype, with prestressing accomplished through adjustments to the truss support and the use of cable net orientation 2.

6.4 Chapter Conclusions

This chapter has described the proof-of-concept demonstrator, which has successfully verified the feasibility of the proposed ISA concept through a series of experimental validations. The entire assembly process was carried out within the truss builder, with each bay constructed and released as planned, and the folded net deployed progressively as more bays were added.

The experiments presented in this chapter have offered valuable insights into the design considerations and their practical effects, serving as critical test cases for comparing with the simulation results presented in Chapters 4 and 5. For the $\theta = 90°$ assembly plate case, the lack of angle stops led to structural distortions and

cable damage, underscoring their importance in maintaining precision. The $\theta = 60^\circ$ case, which included angle stops and a minimal interference gravity offload system, achieved a more controlled and symmetrical deployment, closely matching simulation predictions. In the $\theta = 72^\circ$ case, selected to improve the working space through trial and error, truss node collinearity matched simulation predictions. However, the issue of undesirable stretching in the cable net, as predicted by the simulations (for $\theta = 90^\circ$ and prestressing through movement of the last bay), was effectively addressed by carefully selecting both the assembly plate orientation and prestressing method.

The prototype reflector, designed for modular assembly by simple robots and manufactured using additive techniques, successfully demonstrated bay construction and release operations. Although the proof-of-concept demonstration of the assembly process is still in progress, the results confirm the viability of the proposed ISA scheme for large mesh reflectors and affirms the qualitative predictions made by two-dimensional simulations. It provides a robust basis for scaling the concept to full-sized applications and future space missions.